Low-Loss Analog and Digital Micromachined Impedance Tuners at the Ka-Band

Hong-Teuk Kim, *Student Member, IEEE*, Sanghwa Jung, Kyungteh Kang, Jae-Hyoung Park, Yong-Kweon Kim, *Member, IEEE*, and Youngwoo Kwon, *Member, IEEE*

***Abstract*—This paper presents new types of analog and digital micromachined impedance tuners. Analog impedance tuners using resonant unit cells realized by tunable micromachined capacitors showed a wide tuning range equivalent to almost two quadrants of the Smith chart with a maximum voltage standing-wave ratio (VSWR) of 21.2 at the Ka-band. Frequency variability is also provided through the use of J-inverters with tunable capacitors. Also presented in this paper is a digital micromachined tuner, where the short-circuited shunt stubs are loaded with microelectromechanical system (MEMS) capacitive switches. The electrical length of the stub and the overall impedance of the tuner are thus controlled according to the switching states of the MEMS capacitors. The digital tuner presented impedance ranges suitable for load impedances of the RF power transistors and showed a high maximum VSWR of 32.3. Compared with the state-of-the art tuners using field-effect transistors, micromachined tuners of this paper show superior VSWR ranges as well as wide impedance ranges. Micromachined tuners are very promising for low-loss tuning of the monolithic circuits as well as for accurate noise and power characterization.**

***Index Terms*—Coplanar waveguide, micromachining technology, transmission line, tuner.**

I. Introduction

MONOLITHIC microwave integrated circuits (MMICs) are well suited to high-volume commercial applications due to the capability of the batch process, which is the key to reduce the process cost and enable mass production. However, there are often cases where the fabricated circuits may not meet the required specifications due to the deviations in the process parameters such as layer thickness and doping concentration. For the case of MMICs, it is virtually impossible to correct the values of each component once the fabrication is finished. The tuning elements like the impedance tuner can be very useful for this purpose [1]. With an on-chip impedance tuner, the circuit elements can be fine-tuned to meet the desired specifications if necessary.

The tuner is also useful for device characterization purposes. For these applications, the tuners can be incorporated directly into a probe tip or MMICs, eliminating any loss between the tuner and test device, resulting in high reflection coefficients at the test device [2], [3]. For example, a field-effect transistor (FET)-based impedance tuner has been developed for noise parameter measurements [2]. Similar tuners have been developed for power applications such as load pull measurement. Ida *et al.* have demonstrated an on-wafer tuning loadpull method, where the load impedances of the FETs were controlled by replacing RF probes and removing airbridges on coplanar waveguide (CPW) lines [3]. This method, however, does not offer repeatable electrical tuning.

The tuners are generally required to meet the following conditions. First, a wide impedance tuning range is required to cover as much impedance range as possible. Second, the loss of the tuner should be low enough to achieve reflection coefficients very close to one. Another useful feature of the tuner is the power handling capability, which is most important when applied to the high-power circuits such as power amplifiers. Conventional tuning elements such as p-i-n diodes and transistors have shown relatively limited loss characteristics, leading to reduced impedance ranges. The nonlinear characteristics of the semiconductor-based tuning elements also limit their use as high-power tuning elements. Micromachining techniques are most effective in this regard. The advantages of micromachined components over FETs or p-i-n diodes for tuning elements are their low-loss performance and lack of measurable intermodulation distortion [4].

In this paper, we propose two types of high-performance micromachined tuners at the Ka-band: analog and digital. Analog tuners showed wide tuning ranges using resonant unit cells. Frequency variability has also been added by employing frequency-tunable resonators. Digital tuners using capacitive microelectromechanical system (MEMS) switches have been developed for high-power applications. Digital tuning using MEMS switches offers accurate and repeatable impedance control by using only two stable states (ON and OFF). The analog tuner showed a maximum voltage standing-wave ratio (VSWR) of 21.2 while digital tuner showed a maximum VSWR of 32.3. To the best of our knowledge, this is the first demonstration of low-loss and wide-range impedance tuners using MEMS technology at the Ka-band.

II. Variable Capacitor

The tuners of this paper employ either analog or digital micromachined variable capacitors as the tuning elements. Micromachined varactors are basically parallel-plate capacitors where the top plate is suspended in the air by cantilever or bridge-type anchors. In the case of analog MEMS varactors, electrostatic force between the top and bottom metal plates changes the distance between the plates, causing the capacitance to vary accordingly. In digital varactors, the ON state is defined when the

Manuscript received April 2, 2001; revised August 27, 2001. This work was supported by the Korean Ministry of Science and Technology under the Creative Research Initiative Program.

The authors are with the Center for 3-D Millimeter-Wave Integrated Systems, School of Electrical Engineering, Seoul National University, Seoul, 151-742, Korea (e-mail: htkim@snu.ac.kr; ykwon@snu.ac.kr).

Publisher Item Identifier S 0018-9480(01)10452-7.

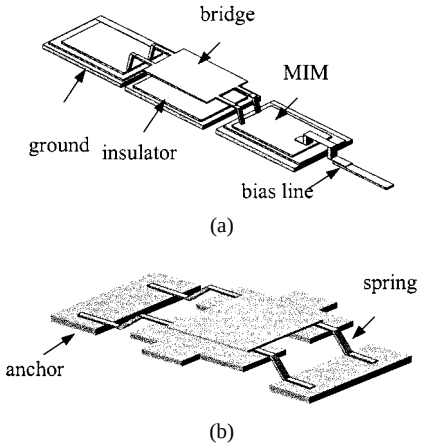

Fig. 1. (a) Shunt capacitor. (b) Series capacitor.

TABLE I
EXTRACTED PARAMETERS OF THE CAPACITOR MODEL

	Rs	Cs	Q
Shunt capacitor OFF	0.25 Ω	61 fF	348
Shunt capacitor ON	0.25 Ω	670 fF	32
Series capacitor OFF	0.5 Ω	26 fF	386
Series capacitor (30% increase)	0.5 Ω	34 fF	295

top plate is completely deflected by applying voltages greater than the pull-in voltage while the OFF state is defined as when the plates are separated as is. Compared with FET or p-i-n diode-based varactors, micromachined varactors offer lower loss and superior linearity characteristics. However, an accurate device model is not available for MEMS varactors. In this paper, varactor model parameters have been extracted for two types of micromachined capacitors used in this study: the shunt capacitor and the series variable capacitor. Fig. 1 shows schematic diagrams of both capacitors.

The two important parameters of variable capacitors are the capacitance ratio ($C\max/C\min$) and the Q-factor. The capacitance ratio determines the tuning range while the Q-factor sets the upper bound for VSWR. To estimate these parameters accurately, one-port varactor test patterns have been fabricated and their S-parameters have been measured up to 100 GHz by on-wafer probing using an HP8510XF vector network analyzer (VNA). The parameters have then been extracted by curve fitting the model to the measured S-parameters. The initial estimate for curve fitting has been calculated by electromagnetic (EM) simulations using IE3D.

Equivalent capacitance and series resistance values have been extracted together with the corresponding Q-factors. Table I shows extracted parameters for each state of the MEMS varactors. The shunt capacitor has been tested under digital driving conditions while the series capacitor has been measured under analog conditions; a 30% change in the capacitance is assumed. The digital shunt capacitor shows a capacitance ratio of 10.9.

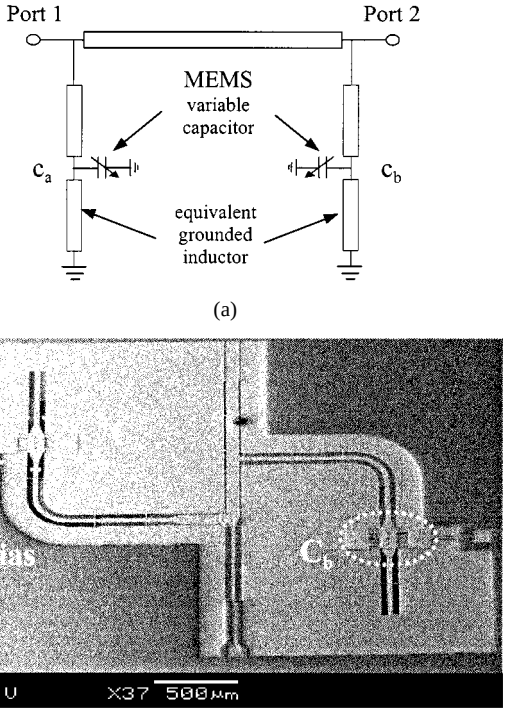

Fig. 2. Fixed-frequency tuner. (a) Schematic. (b) Photograph.

The Q-factor of both capacitors in the OFF state is higher than 340 at 30 GHz.

III. ANALOG IMPEDANCE TUNER

Analog impedance tuners have been realized using tunable metal–air–metal parallel-plate capacitors fabricated by micromachining techniques. It shows a 30% capacitance variation before the top plate of the capacitor is fully deflected. Two types of tunable capacitors were used in the analog tuner: shunt and series.

Since the capacitance variation available from the micromachined capacitor is limited to 30%, a special technique is needed to extend the impedance tuning range needed for tuner operation. For this purpose, we have employed a resonant unit cell operating near the resonance frequency. The large reactance change near the resonant frequency makes it possible to obtain a relatively large impedance variation. Two different analog tuners have been designed and fabricated: the fixed-frequency tuner and the frequency-variable tuner using J-inverters.

A. Fixed-Frequency Tuner Using Shunt Resonant Cells

The schematic and photograph of the fixed-frequency tuner are shown in Fig. 2, which is implemented by the transmission lines loaded with two shunt resonant cells consisting of a micromachined shunt-type variable capacitor and a high-impedance short-circuited line operating as a grounded inductor. The fixed-frequency tuner synthesizes the impedance on the Smith chart by tuning the capacitance of the shunt resonator with the tunable capacitors C_a and C_b. The tuning range of this tuner is targeted for noise matching of the transistors.

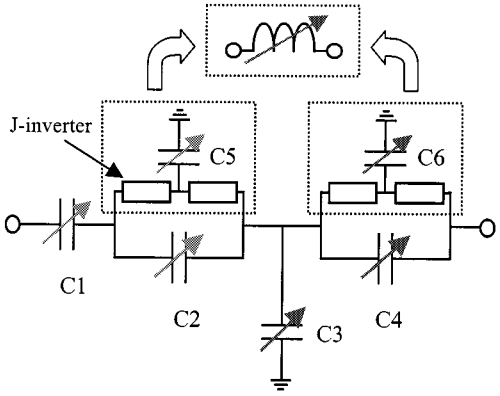

(a)

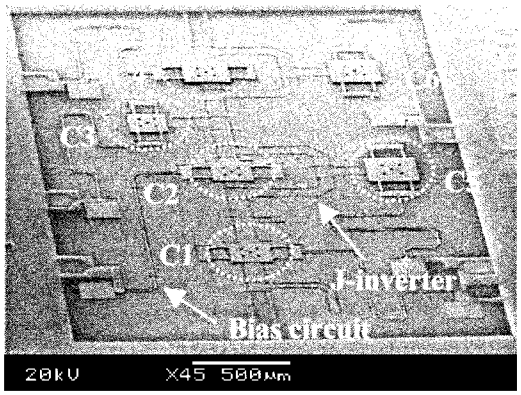

(b)

Fig. 3. Frequency-variable tuner. (a) Schematic. (b) Photograph.

B. Frequency-Variable Tuner Using Resonant Cells With J-Inverters

Even though the resonance-type tuners show a wide impedance range, the operating bandwidth turns out to be very narrow. In order to solve this problem, an additional frequency tuning element is added in the unit cell to change the resonance frequency of the resonator itself. Variable inductors, which are hard to implement in monolithic form, would be needed for this frequency tuning. In this study, an artificial tunable inductor has been synthesized by using a circuit consisting of a shunt-tunable capacitor between two J-inverters [5], [6]. It is then possible to move the resonance frequency with this equivalent variable inductor.

The second design is the frequency-variable impedance tuner shown in Fig. 3. The schematic of the frequency-variable tuner is shown in Fig. 3(a). It consists of two frequency-variable parallel resonant cells and two tunable capacitors ($C1$ and $C3$). The series capacitor $C1$ effectively changes the angle of the reflection coefficient while the parallel resonance cells change the magnitude of the reflection coefficients. Frequency tuning of the resonance cells is achieved by changing the capacitance $C2$ and $C4$ together with the effective inductance with $C5$ and $C6$ connected by J-inverters. The bias circuit to each tunable capacitor is implemented with a quarter-wavelength line and an MIM capacitor. This impedance tuner is designed to synthesize the impedances in the second and third quadrants of the Smith chart for use in the optimum load measurement for power transistors.

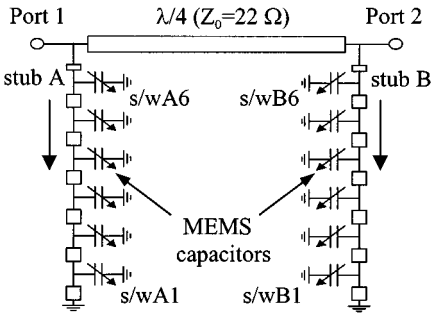

(a)

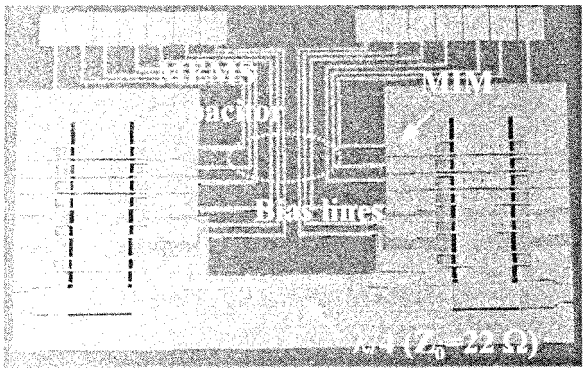

(b)

Fig. 4. Digital MEMS tuner. (a) Schematic. (b) Photograph.

The chip sizes of the fixed-frequency tuner and frequency tunable tuner are 3.2×2.7 mm^2 and 3.7×2.0 mm^2, respectively.

A commercial circuit simulator (HPADS) and an EM simulator (IE3D) have been used for tuner design and analysis. Full-wave analysis has been performed for accurate prediction of tunable parallel-plate capacitors and discontinuities in the CPW.

IV. Digital Impedance Tuner

Digital tuning using MEMS bridge capacitors offers accurate impedance control since it uses only two stable states (ON and OFF states). A digital MEMS tuner was designed to cover the second quadrant of the Smith chart that corresponds to the general impedance area for optimum load matching of power transistors. Fig. 4(a) shows the simplified schematic diagram of the digital MEMS tuner. Two shunt short-circuited stubs loaded with MEMS capacitors are connected to each end of a $\lambda/4$-long series low-impedance line ($Z_0 = i\Omega$). The low Z_0-line (22 Ω) is selected to transform the port-2 impedance of 50 Ω into 10 Ω seen at port 1, offering the synthesized impedances with the presumed optimum load impedance (10 Ω). Here, the 22-Ω line is obtained with the inverted overlay CPW line [7] instead of the conventional CPW lines since the lowest impedance achievable from the latter is higher than the required impedance. To synthesize the tuner impedances, the electrical-length-variable stub lines loaded with the MEMS bridge capacitors in Fig. 1(a) are employed. By switching on the MEMS capacitive switches along the stubs, the shunt capacitance and thus the electrical length of the line are increased, resulting in subsequent impedance change. Switching the MEMS capacitors on one

stub (stub A) of the tuner moves the impedance seen at port 1 in an orthogonal direction compared to the case of switching the MEMS capacitors on the other stub (stub B). This is due to the fact that the $\lambda/4$-long series line functions as a J-inverter. The orthogonality in the impedance change allows uniformly distributed impedances in the tuning area.

In the OFF state, the MEMS bridge is suspended in the air by 2 μm over the stub lines. The size of the MEMS bridge plate is 90 $\times$ 300 μm^2 and the width of the stub line is 300 μm. For biasing each MEMS bridge capacitor, the spring beams of each MEMS bridge and bias lines are connected to the isolated MIM capacitors. Fig. 4(b) is the photograph of the fabricated digital MEMS tuner in which six MEMS switches are inserted into each short-circuited stub. The total chip size is 3 $\times$ 2 mm^2, including the dc bias network and pads for on-wafer measurement. The electrical characteristics of the MEMS bridge capacitor in the ON and OFF states and discontinuities are analyzed by EM software IE3D.

V. Fabrication of the Impedance Tuner

The designed impedance tuners were fabricated on a 520-μm-thick quartz substrate using the surface micromachining technology. The CPW lines, MIM capacitors, and overhanging structures such as variable parallel-plate capacitors and air bridges are formed using the gold electroplating process and subsequent releasing technique.

First, titanium and gold layers are thermally evaporated on the substrate as the seed layer for gold electroplating. Electroplating mold (3.5-μm thick) is patterned with photoresist, through which the CPW transmission lines and bottom plates of the parallel-plate capacitors are electroplated. After electroplating of the first metal, a 0.2-μm-thick dielectric (SiO_2) layer is deposited for the insulating layer of the capacitors. The photoresist sacrificial layer is spin-coated and patterned by UV lithography. The patterned sacrificial layer is thermally cured for reflowing the edge of the photoresist. By curing photoresist, it is chemically stabilized and not affected by the next fabrication steps. Thanks to the shape of the reflowed sacrificial layer, the top plate of the tunable capacitor shows the curved anchor support, which also facilitates the subsequent electroplating steps. Next, the seed layer is evaporated, followed by electroplating of the second metal layer with a thickness of 2 μm for the top plates of the variable capacitors, MIM capacitors, and air bridges. Finally, by removing the sacrificial layer using the plasma ashing process, the overhanging structures suspended over the bottom metal layer can be obtained.

VI. Experimental Results

The measurement of the fabricated impedance tuners was performed by on-wafer probing using an HP 8510C network analyzer. The measured constellation of the impedance points synthesized by the analog fixed-frequency tuner is shown in Fig. 5. The measurement frequency is 29 GHz. It can be seen that the use of the micromachined tuner allows high values of the reflection coefficient to be synthesized over the first and second quadrants of the Smith chart. Fig. 6 shows the measured S_{21} and S_{11} of the fixed-frequency tuner for various bias voltage states at 29 GHz. Bias voltages for each MEMS varactor were 0, 15, 20, 25, and 30 V.

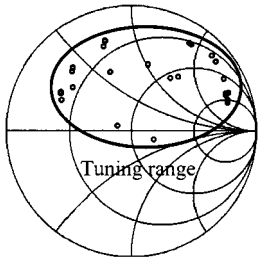

Fig. 5. Measured constellation of the fixed-frequency tuner (frequency = 29 GHz).

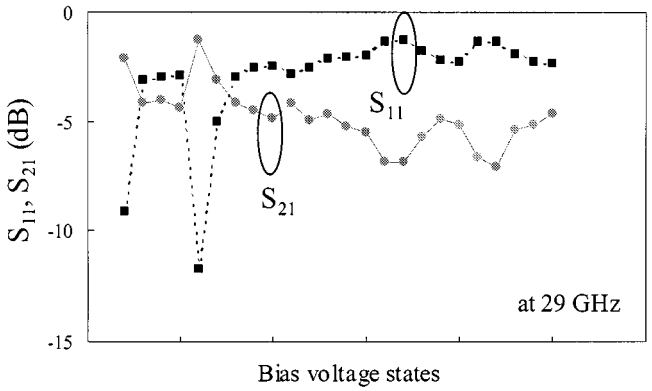

Fig. 6. Measured S_{21} and S_{11} of the fixed-frequency tuner for various bias voltage states (frequency = 29 GHz). Bias voltages of the two MEMS varactors are 0, 15, 20, 25, 30 V.

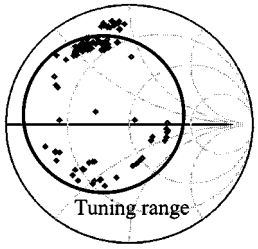

(a)

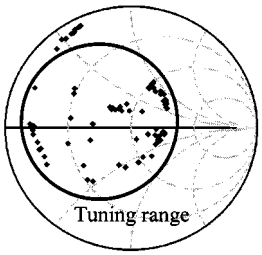

(b)

Fig. 7. Measured constellation of the frequency-variable tuner: (a) before frequency variation (frequency = 25 GHz) and (b) after frequency variation (frequency = 23.5 GHz).

The measured constellation of the impedance points synthesized using the frequency-variable tuner is shown in Fig. 7. As shown in the measured results of Fig. 7(a), the frequency tunable tuner operating at 25 GHz is capable of generating the impedances in the second and third quadrants of the Smith chart,

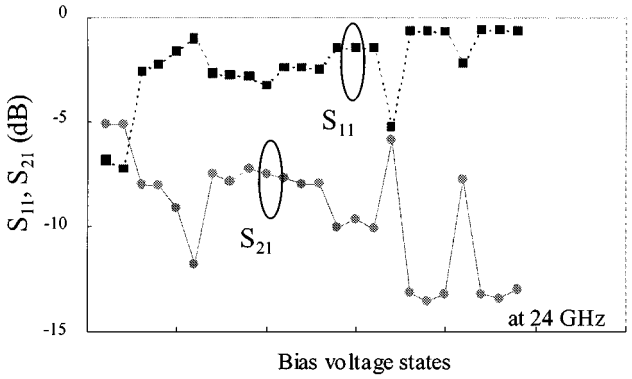

Fig. 8. Measured S_{21} and S_{11} of the frequency-variable tuner for various bias voltage states (frequency = 24 GHz). Bias voltages of six MEMS varactors are between 0 and 40 V in 10-V steps.

which correspond to the optimum load range of the power transistors. To show the frequency variability, the values of $C5$ and $C6$ have been adjusted to shift the resonant frequency from 25 to 23.5 GHz. The constellation of the impedance points measured at 23.5 GHz is shown in Fig. 7(b). The control voltages to each MEMS varactor were linearly distributed from 0 to 40 V in 10-V steps. An impedance range comparable to that at 25 GHz was observed, demonstrating the frequency variability. However, the measured results in Fig. 7 show nonuniformly distributed constellation of the impedance points, which can be understood from the fact that the capacitance of the MEMS varactor does not vary linearly, resulting in uneven capacitance values under even control bias applications. In addition, uniformity issues during the fabrication of the MEMS varactors can also lead to nonuniform constellations.

Fig. 8 shows the measured S_{21} and S_{11} of the frequency-variable tuner for various bias voltage states at 24 GHz. Bias voltages of six MEMS varactors are between 0 and 40 V in 10-V steps.

Fig. 9 shows the measured reflection coefficient traces seen at port 1 of the digital tuner according to each switching state of the MEMS capacitors between 25 and 35 GHz. Initially, all MEMS capacitors are in the OFF-state (A0B0). As the sixth MEMS capacitor on stub A is switched on (from A0 to A6 state), the electrical length of the short-circuited stub A increases by up to 60° (at 30 GHz) at the A6 state. Here, A6 means that only the sixth MEMS capacitor on stub A is switched on and the other MEMS capacitors of both stubs A and B are in the OFF-state. The resulting change in the reflection coefficient at 30 GHz is shown in Fig. 9(a). Impedance traces moves outward from the A0B0 state, making the radius of the circle larger. Fig. 9(b) shows the variation of the reflection coefficient traces according to switching states from B0 to B6 of the MEMS capacitors on stub B. Contrary to Fig. 9(a), the impedance traces move inward from the initial state (A0B0). The impedance points at a fixed frequency move in the orthogonal direction in the case of switching MEMS capacitors on stub A, as expected.

Fig. 10 shows the measured constellation (49 points) of impedances synthesized by the digital MEMS tuner at 29, 30, and 32 GHz at which the tuned impedances are shown to cover the general load-matching area of the RF power transistors. The maximum VSWR achieved by this tuner was as high as 32.3

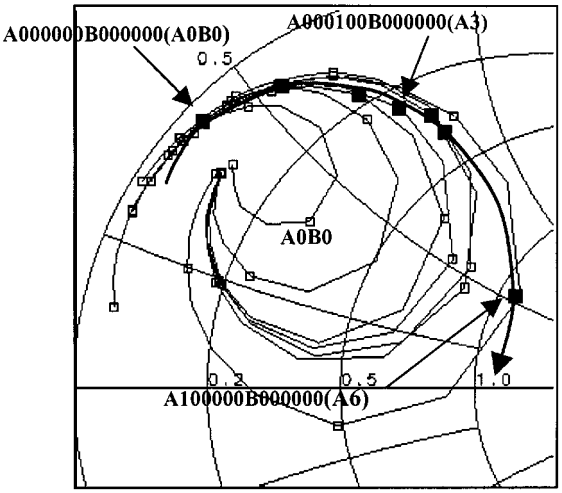

(a)

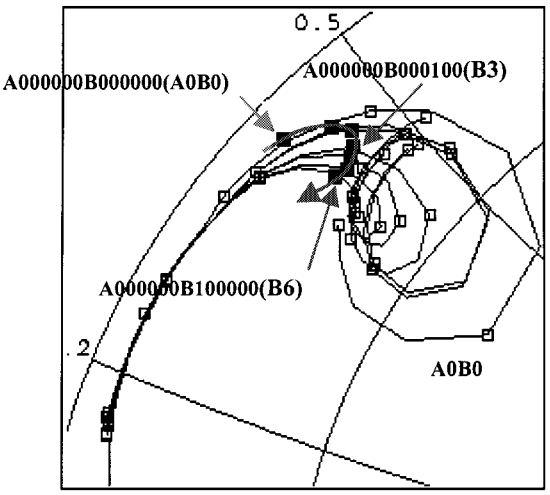

(b)

Fig. 9. Measured reflection coefficient traces of the digital MEMS tuner according to switching states on: (a) stub A and (b) stub B between 25 and 35 GHz. Dark points are the impedance traces at 30 GHz.

at 30 GHz. Fig. 11 shows measured S_{21} and S_{11} of the digital MEMS tuner for various switching states from A0B0 to A6B6 at 30 GHz. The switching voltage is 40 V. In order to verify the usefulness of the digital MEMS tuners for power applications, the power characteristics of the MEMS switches used in the digital tuner were also measured. Fig. 12 shows measured output power versus the input power for the MEMS switch [see Fig. 1(a)] under the "switch-off" state. The MEMS switch shows good linearity up to an input power of 2.2 W at 2 GHz. Here, we used a 2-GHz RF source instead of the Ka-band source due to the limited output power range of the latter (<1 W). However, the results should be very similar at higher frequencies.

In Table II, the measured VSWR data of the two types of micromachined impedance tuners of this study are compared with other reported tuner data using high electron-mobility transistor (HEMT) switches. It can be seen that the micromachined impedance tuners exhibit a superior VSWR compared to that of the conventional tuners using FETs, which is attributed to the low-loss nature of the micromachined components. This clearly shows the advantage of the micromachined tuners.

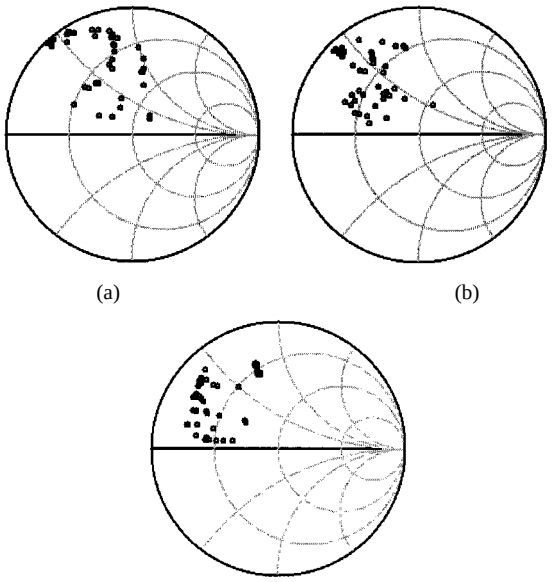

Fig. 10. Measured constellation (49 points) of the digital MEMS tuner at: (a) 29, (b) 30, and (c) 32 GHz.

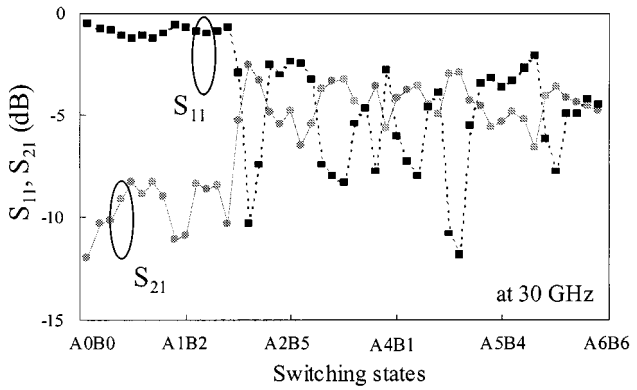

Fig. 11. Measured S_{21} and S_{11} of the digital MEMS tuner for various switching states from A0B0 to A6B6 (frequency $=$ 30 GHz). The switching voltage is 40 V.

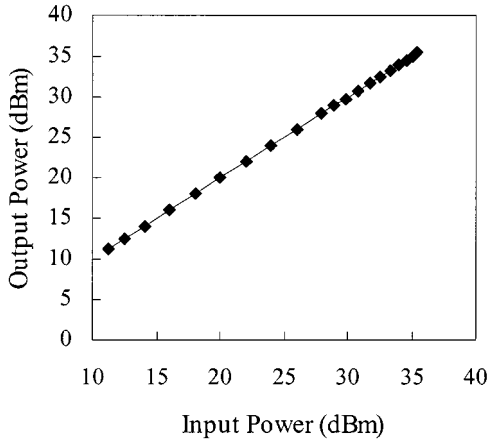

Fig. 12. Characteristics of the power capability of the MEMS switch [see Fig. 1(a)] on the digital MEMS tuner. The measured frequency is 2 GHz.

TABLE II
COMPARISON OF MEASURED VSWR WITH OTHER REPORTED DATA

Tuner type	VSWR	Frequency	Ref.
Frequency fixed tuner	14.4	29 GHz	this work
Frequency tunable tuner	21.2	25 GHz	this work
Digital tuner	32.3	30 GHz	this work
HEMT tuner	6	27 GHz	[1]
HEMT tuner	12.3	18 GHz	[2]

VII. CONCLUSION

In this paper, analog and digital impedance tuners are designed and fabricated with micromachining techniques. The analog impedance tuners used the resonant unit cell for wide tuning ranges. Even with the limited capacitance variations available from the micromachined tunable capacitors (∼30%), a wide tuning range was achieved with the help of the resonant unit cells. The narrow bandwidth of the resonant-type tuners has also been alleviated by employing tunable unit cells realized by artificial tunable inductors using J-inverters and tunable capacitors. Measured micromachined tuners showed a wide tuning range equivalent to almost two quadrants with a high maximum VSWR of 21.2 at 25 GHz.

The digital tuner has been proven to achieve a wide impedance range in the general load-matching area of the RF power transistors by using the switchable bridge-type MEMS capacitors. The digital tuning approach allows immunity to bias voltage fluctuations and enhances power handling capability. In the digital MEMS tuner, switching the MEMS capacitors changed the electrical length of the short-circuited stubs, resulting in impedance variation. The measured constellation of impedances synthesized by the digital MEMS tuner covered the second quadrant on the Smith chart, the general load-matching area of RF power transistors at 29∼32 GHz. A high maximum VSWR of 32.3 was achieved at 30 GHz.

These VSWR numbers are far greater than those of the comparable tuners using HEMT devices. Micromachined tuners are very promising for low-loss/high-Q tuning of the circuits, as well as for accurate noise and power measurements at millimeter waves.

REFERENCES

[1] W. Bischof, "Variable impedance tuner for MMICs," *IEEE Microwave Guided Wave Lett.*, vol. 4, pp. 172–174, June 1994.
[2] C. E. McIntosh, R. D. Pollard, and R. E. Miles, "Novel MMIC source-impedance tuners for on-wafer microwave noise-parameter measurements," *IEEE Trans. Microwave Theory Tech.*, vol. 47, pp. 125–131, Feb. 1999.
[3] M. Ida and M. Nakatsugawa, "Design of a K-band power amplifier of using on-wafer-tuning load–pull method," *IEICE Trans. Electron.*, vol. E81-C, no. 6, pp. 882–885, June 1998.
[4] C. Goldsmith, J. Randall, S. Eshelman, T. H. Lin, D. Dennistor, S. Chen, and B. Norvell, "Characteristic of micromachined switches at microwave frequencies," in *IEEE Microwave Theory Tech. Symp. Dig.*, June 1996, pp. 1141–1144.
[5] J. H. Sinsky and C. R. Westgate, "Design of an electronically tunable microwave impedance transformer," in *IEEE Microwave Theory Tech. Symp. Dig.*, June 1997, pp. 647–650.

[6] G. Matthaei, L. Young, and E. M. T. Jones, *Microwave Filters, Impedance-Matching Networks, and Coupling Structure*. Norwood, MA: Artech House, 1980, pp. 434–438.
[7] Y. Kwon, H. T. Kim, J. H. Park, and Y. K. Kim, "Low-loss micromachined inverted overlay CPW lines with wide impedance ranges and inherent airbridge connection capability," *IEEE Microwave Wireless Components Lett.*, vol. 11, pp. 59–61, Feb. 2001.

Hong-Teuk Kim (S'99) was born in Pusan, Korea, in 1968. He received the B.S. degree from Pusan National University, Pusan, Korea, in 1991, the M.S. degree in electrical engineering from the Korea Advanced Institute of Science and Technology (KAIST), Taejon, Korea, in 1993, and is currently working toward the Ph.D. degree at the at Seoul National University, Seoul, Korea.

From 1993 to 1998, he was with the LG Central Institute of Technology (LGCIT), where he was engaged in low-noise system integration and superconductor RF filter design for wireless application. His current research is focused on MMIC design, RF MEMS design, and analysis of oscillator phase noise.

Sanghwa Jung was born in Korea, in 1973. He received the B.S. degree from Seoul National University, Seoul, Korea, in 1999, and is currently working toward the M.S. degree at Seoul National University.

His current research activities include the design of MMICs for microwave and millimeter-wave systems and the application of micromachining techniques to millimeter-wave systems.

Kyungteh Kang was born in Korea, in 1977. He received the B.S. degree from the Seoul National University, Seoul, Korea, in 2000, and is currently working toward the M.S. degree at Seoul National University.

His current research activities include the design of spatial power combining circuits in the millimeter-wave region and MEMS application.

Jae-Hyoung Park received the B.S. and M.S. degrees from Seoul National University, Seoul, Korea, in 1997, 1999 respectively, and is currently working toward the Ph.D. degree in electrical engineering at Seoul National University.

He is currently with the Electroplating Micromachining Group, Micro Sensors and Actuators Laboratory, Seoul National University. From 1997 to 1998, his main research activities were focused on manipulation of the micro particle. Since 1998, his research topic has been the design and fabrication of RF MEMS devices.

Yong-Kweon Kim (S'90–M'90) received the B.S. and M.S. degrees in electrical engineering from Seoul National University, Seoul, Korea, in 1983 and 1985, respectively, and the Dr.Eng. degree from the University of Tokyo, Tokyo, Japan, in 1990. His doctoral dissertation was on modeling, design, fabrication, and testing of micro linear actuators in magnetic levitation using high critical temperature superconductors.

In 1990, he joined the Central Research Laboratory, Hitachi Ltd., Tokyo, Japan, as a Researcher and was involved with actuators of hard disk drives. In 1992, he joined Seoul National University, where he is currently an Associate Professor in the School of Electrical Engineering. His current research interests are modeling, design, fabrication, and testing of electric machines, especially micro electromechanical systems, micro sensors, and actuators.

Youngwoo Kwon (S'90–M'94) was born in Korea, in 1965. He received the B.S. degree in electronics engineering from Seoul National University, Seoul, Korea, in 1988, and the M.S. and Ph.D. degrees in electrical engineering from The University of Michigan at Ann Arbor, in 1990 and 1994, respectively.

From 1994 to 1996, he was with Rockwell Science Center, where he was involved in the development of various millimeter-wave monolithic integrated circuits based on HEMTs and HBTs. In 1996, he joined the faculty of the School of Electrical Engineering, Seoul National University. His current research activities include the design of MMICs for mobile communication and millimeter-wave systems, large-signal modeling of microwave transistors, application of micromachining techniques to millimeter-wave systems, nonlinear noise analysis of MMICs, and millimeter-wave power combining.